Received: 15 June 2019 | Revised: 12 July 2019 | Accepted: 25 July 2019

DOI: 10.1002/inf2.12033

ORIGINAL ARTICLE

WILEY

Space-confined microwave synthesis of ternary-layered BiOCl crystals with high-performance ultraviolet photodetection

Lixing Kang[1,2] | Xuechao Yu[3] | Xiaoxu Zhao[5] | Qingling Ouyang[2,3] | Jun Di[1] | Manzhang Xu[1] | Dan Tian[1] | Weiliang Gan[4] | Calvin C. I. Ang[4] | Shoucong Ning[5] | Qundong Fu[1] | Jiadong Zhou[1] | R. G. Kutty[1] | Ya Deng[1] | Pin Song[1] | Qingsheng Zeng[1] | Stephen J. Pennycook[5] | Jun Shen[6] | Ken-T. Yong[2,3] | Zheng Liu[1]

[1]School of Materials Science and Engineering, Nanyang Technological University, Singapore

[2]CINTRA CNRS/NTU/THALES, Singapore

[3]Centre for OptoElectronics and Biophotonics, School of Electrical and Electronic Engineering, Nanyang Technological University, Singapore

[4]School of Physical and Mathematical Sciences, Nanyang Technological University, Singapore

[5]Department of Materials Science and Engineering, National University of Singapore, Singapore

[6]Chongqing Institute of Green and Intelligent Technology, Chinese Academy of Sciences, Chongqing, China

Correspondence
Jun Shen, Chongqing Institute of Green and Intelligent Technology, Chinese Academy of Sciences, Chongqing, China.
Email: juns@cigit.ac.cn

Ken-T. Yong, CINTRA CNRS/NTU/THALES, UMI 3288, Research Techno Plaza, 50 Nanyang Drive, Border X Block, Singapore.
Email: ktyong@ntu.edu.sg

Zheng Liu, School of Materials Science and Engineering, Nanyang Technological University, 50 Nanyang Avenue, Singapore.
Email: z.liu@ntu.edu.sg

Abstract

In recent years, two-dimensional (2D) ternary materials have attracted wide attention due to their novel properties which can be achieved by regulating their chemical composition with a very great degree of freedom and adjustable space. However, as for the precise synthesis of 2D ternary materials, great challenges still lie ahead that hinder their further development. In this work, we demonstrated a simple and reliable approach to synthesize 2D ternary-layered BiOCl crystals through a microwave-assisted space-confined process in a short time (<3 minutes). Their ultraviolet (UV) detection performance was analyzed systematically. The photodetectors based on the as-obtained BiOCl platelets demonstrate high sensitivity to 266-nm laser illumination. The responsivity is calculated to be ~8 A/W and the response time is up to be ~18 ps. On the other hand, the device is quite stable after being exposed in the ambient air within 3 weeks and the response is almost unchanged during the measurement. The facile and fast synthesis of single crystalline BiOCl platelets and its high sensitivity to UV light irradiation indicate the potential optoelectronic applications of 2D BiOCl photodetectors.

KEYWORDS

2D materials, bismuth oxyhalide, microwave synthesis, UV photodetector

Lixing Kang, Xuechao Yu, and Xiaoxu Zhao contributed equally to this work.

This is an open access article under the terms of the Creative Commons Attribution License, which permits use, distribution and reproduction in any medium, provided the original work is properly cited.

© 2019 The Authors. *InfoMat* published by John Wiley & Sons Australia, Ltd on behalf of UESTC.

Funding information
National Research Foundation Singapore, Grant/Award Numbers: A*Star QTE program., AcRF Tier 2 MOE2017-T2-2-002, MOE Tier 2 MOE2015-T2-2-007, MOE Tier 3 MOE2018-T3-1-002, MOE2016-T2-2-153, MOE2017-T2-2-136, NRF-RF2013-08. MOE Tier 1 RG7/18, NRF2017-NRF-ANR002 2DPS; Natural Science Foundation of Jiangsu Province, Grant/Award Number: BK20160994

1 | INTRODUCTION

Since the discovery of graphene, much academic attention has been drawn to the nanoscale in the materials realm.[1,2] In the near past, this intriguing type of material has been recognized and termed distinguishingly as two-dimensional (2D) materials. The family of 2D materials has grown, displaying a broad range of unique properties.[3,4] Recently, in a rather attractive direction, 2D ternary materials have drawn more and more attention and thoughts.[5,6] Compared with 2D binary compounds, three-element 2D materials have more freedom to tailor their chemical and physical properties through the variation of element species. To date, some exciting properties have been successfully found in 2D ternary-layered compounds, including excitonic insulating phase in Ta_2NiSe_5,[7] high electron mobility in Bi_2O_2Se,[8] and intrinsic ferromagnetism in $Cr_2Ge_2Te_6$ and Fe_3GeTe_2.[9,10] Photodetectors based on the $Ga_2In_4S_9$ flakes also display an excellent performance.[11] In order to expand the family of 2D ternary materials and investigate their special properties, exploring new ternary-layered compounds and developing reliable synthetic methods are extremely urgent and necessary.

As a new layered ternary material, bismuth oxyhalide BiOX (X = Cl, Br, and I) has attracted a great deal of concern and interest in the field of photocatalytic energy conversion and environmental remediation in recent years.[12] Barium oxyhalide is a typical multicomponent metal halide oxide, which belongs to group V-VI-VII, with high chemical stability, nontoxicity, and corrosion resistance.[13,14] Most recently, Feng et al[15] have reported a facile synthesis of large-area atomically thin BiOI by space-confined chemical vapor deposition (CVD), and for the first time attempted a visible light photodetector based on 2D BiOI nanosheets with good photo response and high sensitivity. Compared with BiOI, BiOCl possesses a relatively big band gap close to 3.2 eV with pronounced photosensitivity, which shows promise for ultraviolet (UV) light detection.[16] Up to now, most of the BiOCl synthesis works focus on the well-developed liquid phase method.[15] The surface contamination and low quality of the BiOCl obtained by hydrothermal obstruct their practical application in photoelectric conversion and semiconductor device areas. Unfortunately, there are also no reports on the growth of 2D ternary BiOCl flakes with controllable stoichiometry on the surface of a flat substrate by CVD method. A detrimental reason is that the common precursors for the synthesis of BiOCl, such as $BiCl_3$ and Bi $(NO_3)_3$ are extremely easy to hydrolyze in air and decompose to bismuth oxide when the control of heating temperature is unsuitable.[17] Unlike conventional CVD heating, microwave heating utilizes polar molecules rotating in the electromagnetic field to realize the conversion of electromagnetic energy to thermal energy.[18,19] Thus, the distinctive character of microwave heating is quick and efficient, which opens the new way to synthesize some special material using microwave technology.

Here, we reported an extremely fast and reliable approach to the synthesis of 2D ternary-layered BiOCl crystals by the space-confined microwave-assisted heating process. The detailed characterizations, including Raman, atomic force microscopy (AFM), X-ray absorption spectra (XPS), and scanning transmission electron microscopy-annular dark field (STEM-ADF), were recorded and confirmed that the as-obtained BiOCl samples were a single crystal with high quality. UV photodetectors based on as-grown 2D BiOCl crystals were also fabricated and showed a highly sensitive detection.

2 | RESULTS AND DISCUSSION

Figure 1A shows the structure models of BiOCl. Its crystal structure belongs to the PbFCl type tetragonal system.[20] BiOCl can also be regarded as a layered structure in which the $[Bi_2O_2]^{2+}$ layer and the double slabs of halogen ions $[Cl]^{-1}$ layer are interlaced in the *c*-axis direction. The inner layer atoms are in the form of strong covalent bonds, while the interlayers are weak van der Waals forces.[16,21] As shown in Figure 1B, the BiOCl crystals were synthesized using an ordinary household microwave oven operating at 2.45 GHz

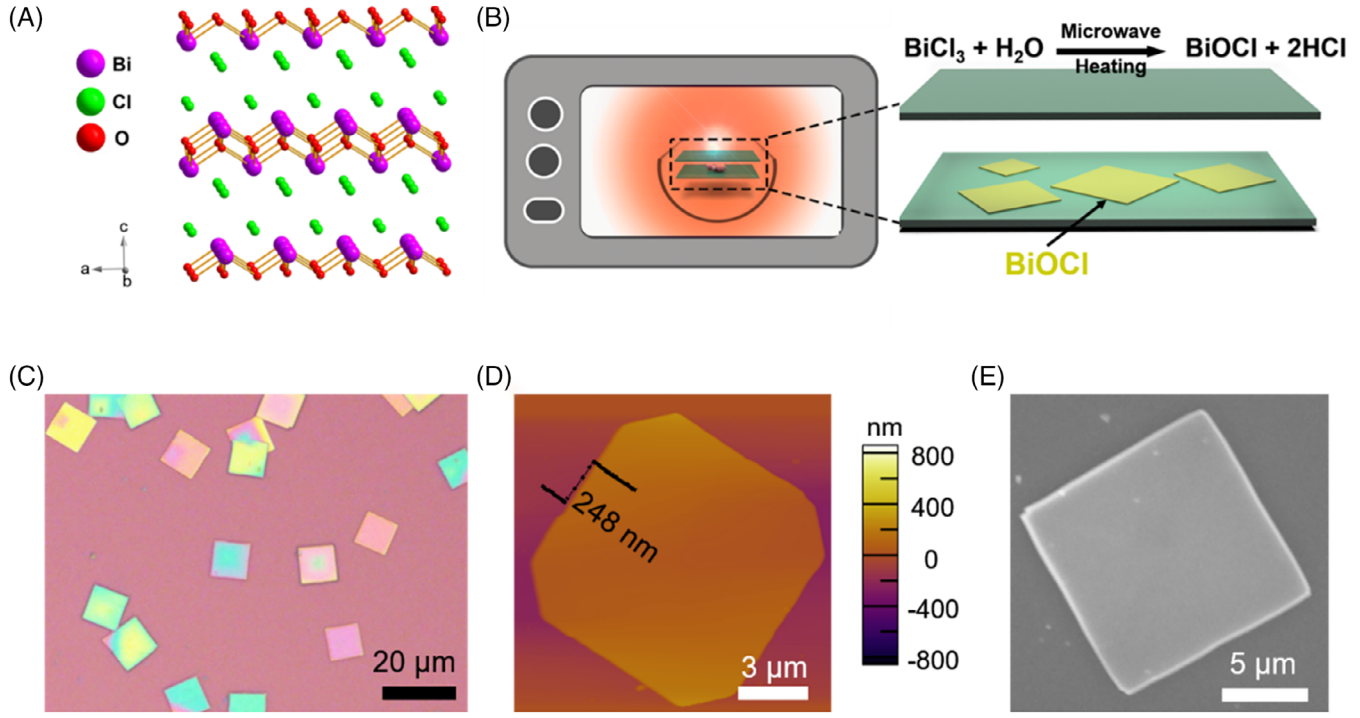

FIGURE 1 A, The schematic of layered crystal structure of BiOCl. B, Schematic illustration of the space-confined microwave synthesis of BiOCl crystals. C, Optical image of square BiOCl flakes on SiO_2/Si substrate. The size is around 10 μm. D, AFM topography of BiOCl crystal and corresponding height profile. E, SEM image of an individual BiOCl nanosheet. AFM, atomic force microscopy; SEM, scanning electron microscope

with 700 W of power. Solid bismuth chloride ($BiCl_3$) powder was chosen as the precursor, which was readily to react with the moisture in the air to form the intermediate hydrate $BiCl_3{\cdot}H_2O$.[17] Two SiO_2/Si substrates were stacked together directly to create a narrow gap and a small amount of $BiCl_3$ powder was located in the confined space.[22,23] Turning on the microwave, the $BiCl_3{\cdot}H_2O$ was heated by a molecular interaction with the electromagnetic field and then decomposed to square shape bismuth oxychloride flakes on the SiO_2/Si substrate. The whole process can be finished within 3 minutes, and the details are described in Section 4. Figure 1C shows a representative optical image of the as-obtained BiOCl crystals grown on the SiO_2/Si substrate. These BiOCl flakes are square-shaped with the edge size up to 10 μm and the usual thickness is about 248 nm according to the AFM image (Figure 1D). The scanning electron microscope (SEM) image of a BiOCl nanosheet (Figure 1E) shows a clean and uniform surface, without granular deposit, indicating a good crystalline morphology. Note that besides SiO_2/Si, other substrates, such as bare silicon and mica, can also be employed (Supporting Information Figure S1). Moreover, the BiOCl crystals grown on the mica show much thinner with the thickness down to 8.7 nm (Figure S1B, C), which could be due to no dangling bonds on the mica surface. The free migration of adatoms on a mica surface is much easier than on SiO_2/Si substrates during the growth.[13] However, the fabrication of devices on insulating mica is often hindered by incompatibility between the silicon technology.[24] So, we focus on the direct growth of BiOCl crystals on SiO_2/Si. In addition, the confined space and growth time are critical factors to obtain uniform BiOCl crystals. When the microwave synthesis process takes place in open space (Figure S2) or prolonged the reaction time to 5 and 8 minutes (Figure S3), the obtained BiOCl crystals become thicker and unhomogeneous. The terraced structures could also be found on some BiOCl crystals.

Further characterizations were performed to investigate the composition and bandgap of the as-obtained BiOCl crystals. In Figure 2A, typical Raman spectra with a 532 nm excitation laser show two obvious resonance peaks at 142 and 198 cm^{-1}, corresponding to the A_{1g} and E_g internal Bi—Cl stretching modes, respectively.[21] The uniform color contrast of Raman mapping image at A_{1g} modes (≈142 cm^{-1}) (inset in Figure 2A) suggests a high quality of the as-grown crystal structure. The characteristic RM peaks at 142 and 198 cm^{-1} are also good consistency with the prior reports,[14,21] implying that high-purity BiOCl crystals have been synthesized. Then, the BiOCl platelets grown on SiO_2/Si substrate were transferred to the fused quartz surface by a PS-assisted method to do the Ultraviolet-Visible (UV-Vis) absorption and X-ray diffraction (XRD) analysis. The detailed transfer process is described in Section 4. As shown in Figure 2B, the band gap value of BiOCl crystals was calculated to be 3.18 eV using a classical Tauc approach

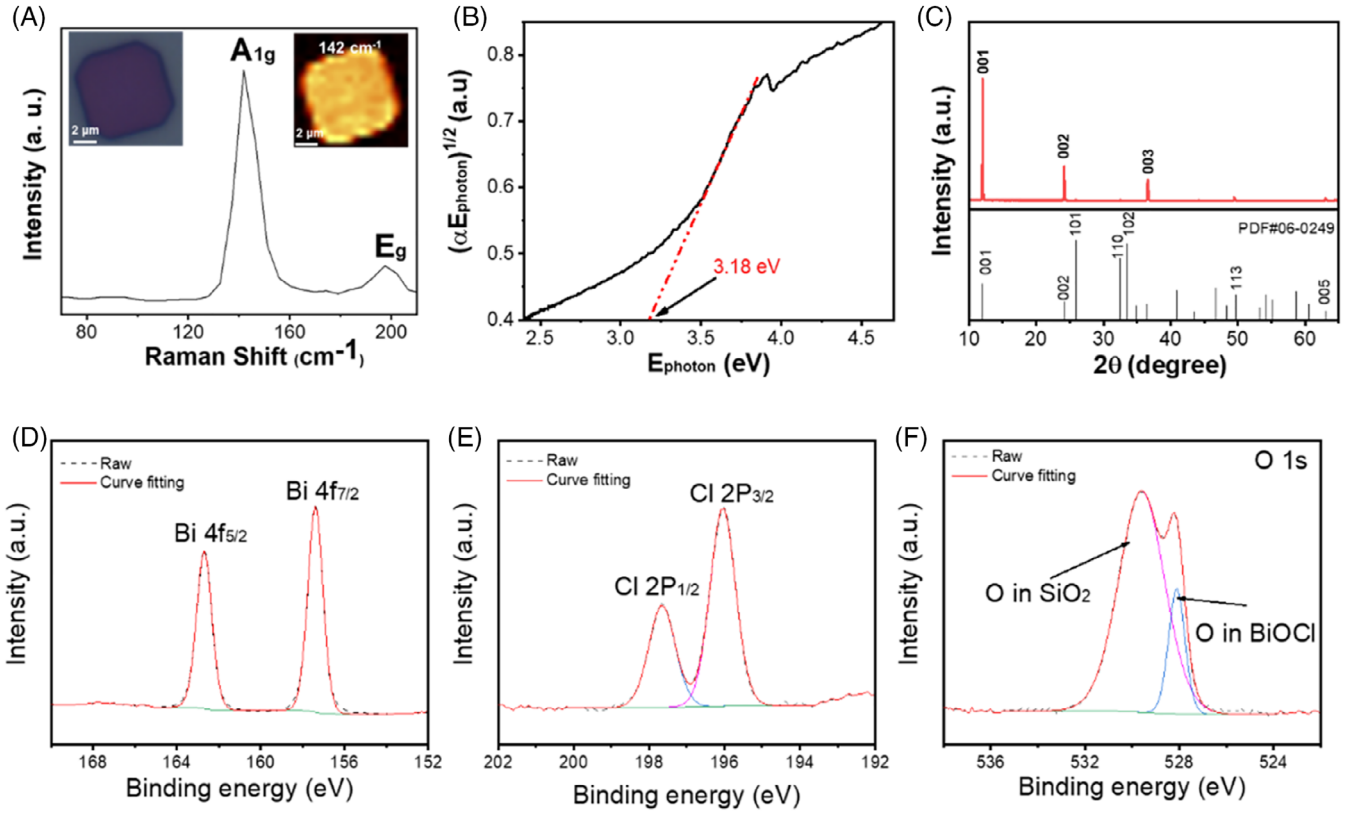

FIGURE 2 A, Typical Raman spectrum of BiOCl nanoplates, the inset shows the optical image of an individual BiOCl platelet and the corresponding Raman mappings at 142 cm^{-1}. B, $(\alpha E_{photon})^{1/2}$ vs E_{photon} curves of the as-prepared BiOCl crystals. α is the absorption coefficient and E_{photon} is the discrete photo energy. C, XRD pattern of BiOCl transferred on a glass slide (red) compared with the standard tetragonal BiOCl pattern (PDF#06-0249) (black). XPS spectr of the BiOCl crystals for Bi 4f D, Cl 2P E, and O 1 second F binding energies. XPS, X-ray photoelectron spectroscopy; XRD, X-ray diffraction

according to its UV-Vis absorption spectra (Figure S2).[25] The XRD pattern of the resulting BiOCl platelets is shown in Figure 2C. Three distinct diffraction peaks are corresponding to the (001), (002), and (003) planes of the tetragonal BiOCl crystals, concluded by the standard tetragonal BiOCl pattern (JCPDS card 06-0249). These diffraction peaks are intense and sharp, indicating that our material is well-crystallized. In addition, all three peaks (001, 002, and 003) are assigned to the (001) family planes, which could be attributed to the [001] direction of the as-obtained crystals is perpendicular to the growth substrate.[20] To investigate the surface states and chemical compositions of the as-grown BiOCl flakes, XPS measurements were carried out. The high-resolution XPS spectra of Bi 4f, Cl 2p, and O 1s are given in Figure 2D-F, respectively. As shown in Figure 2D, a typical $4f_{7/2}$ (157.4 eV) and $4f_{5/2}$ (162.7 eV) doublet in Bi 4f spectra are accounted for by the spin-orbit coupling effect, which shows good consistency with the reported values for BiOCl powders.[20] Two characteristic peaks for chloride anions at 196.0 and 197.7 eV in Cl 2p (Figure 2E) are assigned to Cl $2p_{3/2}$ and Cl $2p_{1/2}$, respectively. The O1s peaks at 528.1 and 529.6 eV are corresponding to the oxygen anions in the Bi—O bond from BiOCl and the oxygen anions in the Si—O bond from SiO_2/Si substrate, respectively.[13] No other doublet found in Bi 4f and Cl 2p spectra and the stoichiometric ratio of Bi/Cl is quite close to 1 indicating that the BiOCl is the high purity phase.

Next, we applied STEM-ADF imaging to investigate the crystallinity of the BiOCl crystals. The contrast of STEM-ADF image is dependent on the Z atomic number as approximately $\sim Z^{1.6\text{-}1.7}$, thereby it was widely employed for analyzing crystal structures and atomic defects in 2D materials.[26,27] From the theoretical atomic model (Figure 3A), we can see that BiOCl crystal shows a perfect tetragonal lattice along the [001] zone axis. All atomic columns are equivalent containing periodic O—Bi—Cl atomic planes. A typical STEM image and its enlarged image of the as-grown BiOCl crystal along the [001] direction are shown in Figure 3B,C. It can be seen that the tetragonal phase contrast patterns are highly homogenous suggesting that the crystal has no noticeable structural defects. Corresponding fast Fourier transform (FFT) pattern (Figure 3D) reveals one set of spots that further corroborate the single crystallinity of BiOCl crystals. In addition, we applied energy dispersive X-ray spectroscopy

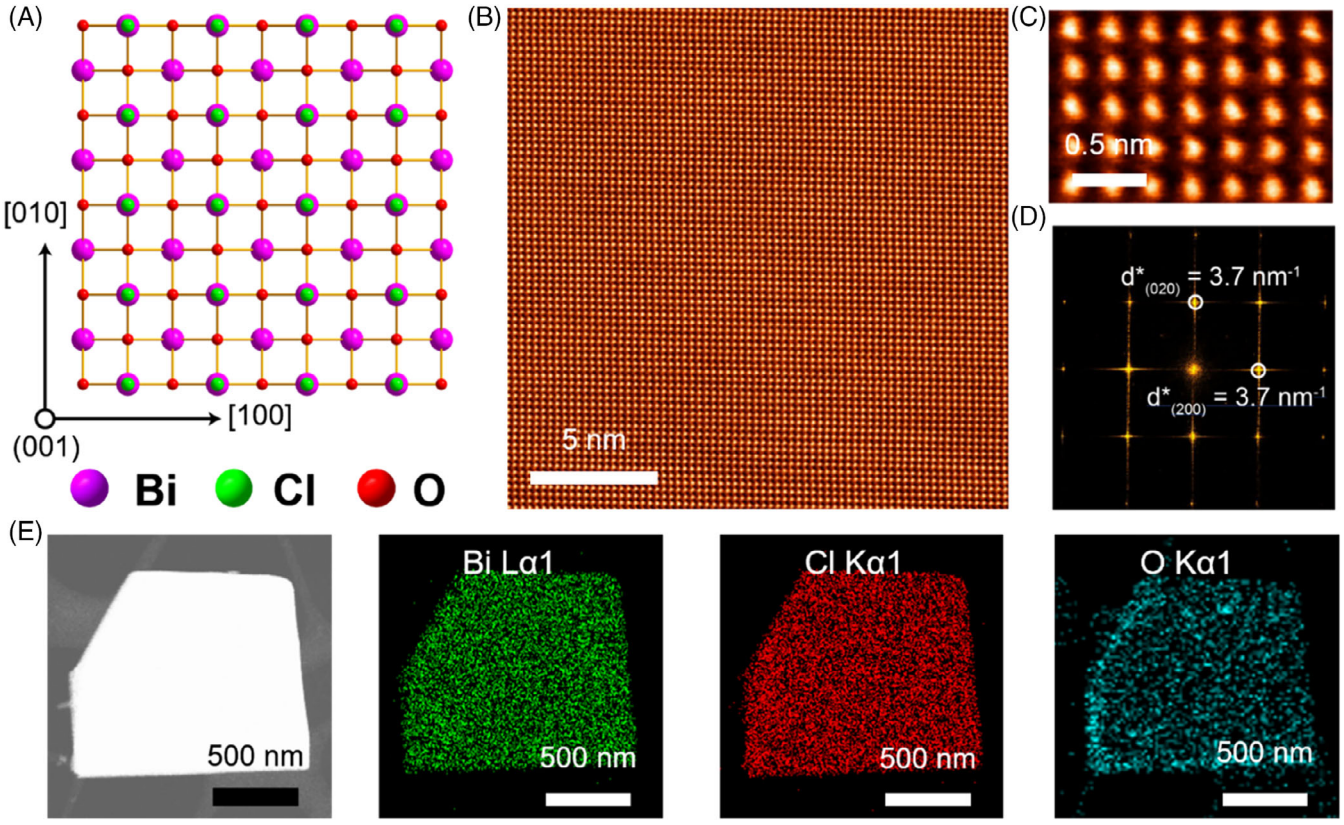

FIGURE 3 STEM characterization of BiOCl crystals. A, Atomic model of BiOCl crystal along the [001] zone axis. B, Atomic-resolution STEM-ADF image of a BiOCl crystal along the [001] direction. C, the enlarged STEM image. D, corresponding fast Fourier transform (FFT) pattern of B. E, EDS mapping of a typical BiOCl crystal. EDS, energy dispersive X-ray spectroscopy; STEM-ADF, scanning transmission electron microscopy-annular dark field

(EDS) mapping (Figure 3E) and found that the distribution of each element is homogenous suggesting that macroscopically the BiOCl is free of large-scale structural defects.

In order to investigate the potential optoelectronics applications of our BiOCl crystals, photodetectors based the individual BiOCl flakes were fabricated on SiO_2/Si substrate. The schematic of the BiOCl detector is a photoconductive field-effect transistor with effective illumination area about 100 μm^2 as shown in Figures S5 and S6. The device fabrication process and more details are described in Section 4. Figure 4A illustrates the energy band diagram of the device under 266 nm laser illumination ($h\nu$ = 4.66 eV) which is adequate to excite the carriers in the valance band to the conduction band. As shown in Figure 4B, the photocurrent increases with the increase in the driven voltage and laser power. The responsivity (R) is calculated to be ~8 A/W under continuous wave 266 nm laser illumination with a driven voltage of 5 V. The result indicates the potential application of BiOCl nanosheet as a UV detector. In order to determine the intrinsic response time of the BiOCl nanosheet, a ~500 ps, 266 nm pulse laser is employed via a two-pulse photocurrent correlation method as described in Section 4. In the experiment, we apply a small driven voltage between the source and drain electrodes to measure the photocurrent together with a lock-in amplifier. The photocurrent is calculated by eliminating the dark current from the current when the light was focused on the sample. The clear dip in the photocurrent curve as shown in Figure 4C indicates fast response of the BiOCl nanosheet between two temporally nearby pulse excitations. It could further evaluate the extraction speed of the photocarriers from the first pulse excitation before the second pulse's arrival.[28,29] When the pump and probe pulses overlap with nearly zero-time delay, the photocurrent is minimum due to the sublinear power-dependent photocurrent. However, when time delay increases, the photocurrent dynamically increases accordingly and saturate when the photocarriers are completely extracted from the pump pulse.[30] The response time is calculated to be ~18 ps with the exponential fitting of the rising curve. We assume that the fast response is originated from the short electron-hole lifetimes in BiOCl.[31] The linear dependence of the photocurrent on the incident laser pulse fluence (Figure 4D) indicates that the number of photogenerated carriers increases with the increase of the incident laser power and also demonstrates that the photocarrier dynamics involved both traps/defects and mid-gap

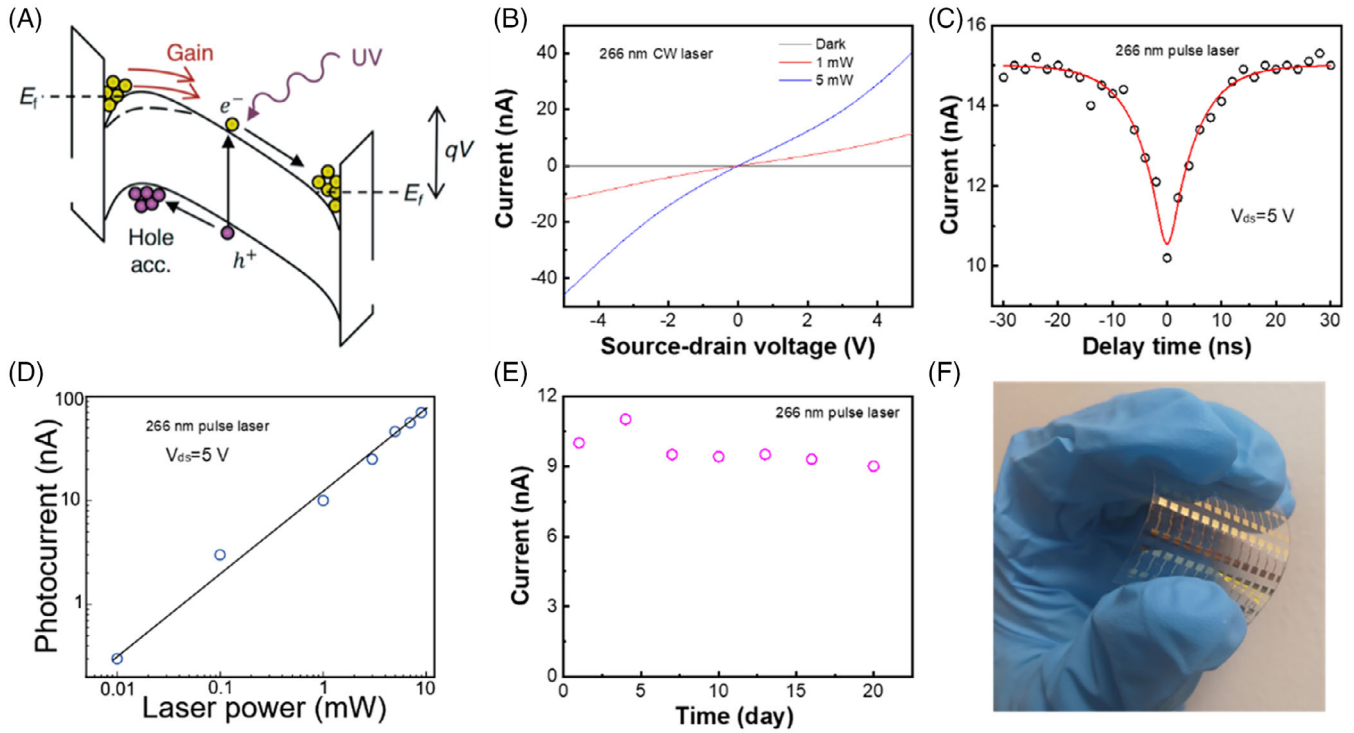

FIGURE 4 A, The energy band diagram of the device under UV light illumination. B, The light response curve of the device under 266 nm laser illumination. C, Time-resolved photocurrent corresponding to the delay time between two pulse lasers at 5 V bias voltage. D, Photocurrent measured at different incident laser pulse influences. E, Stability of BiOCl detector measured in air for 3 weeks. F, Photograph of the BiOCl detector arrays transferred on the PDMS substrate. UV, ultraviolet; PDMS, polydimethylsiloxane

states.[32] Further investigation is required to interpret the complex-carrier recombination and scattering processes of the photogenerated electron/hole pairs under UV laser illumination. On the other hand, the device is quite stable after being exposed in ambient air within 3 weeks and the response is almost unchanged during the measurement as shown in Figure 4E, indicating the potential applications of the 2D BiOCl photodetectors. For example, the detector arrays can be transferred to a polydimethylsiloxane substrate by a facial method (Figure 4F), which is promising for wearable UV detector for daily UV illumination monitor.

3 | CONCLUSIONS

In conclusion, we reported a space-confined microwave synthesis of single crystalline tetragonal BiOCl platelets. Contrary to the traditional CVD process, the microwave-assisted heating process shows an extremely fast growth of few-layer BiOCl within 3 minutes in air. Through XRD, XPS, and HRTEM studies, we confirmed the single phase of BiOCl. The BiOCl-based UV photodetector exhibits an excellent performance with high responsivity and fast response characteristic. We assume that the fast response is originated from the short electron-hole lifetime in high crystalline quality BiOCl flakes. The mild growth conditions and excellent UV detection performance of BiOCl suggest that 2D BiOCl is a promising material for optoelectronic applications and other fundamental properties investigations. Furthermore, our microwave-assisted heating process offers more choices for the structure-control growth of other atomically 2D materials due to the simplicity and speediness of the process.

4 | EXPERIMENTAL SECTION

4.1 | Microwave synthesis of BiOCl crystals

The microwave synthesis process is schematically depicted in Figure 1B. In detail, the primary equipment is a conventional household microwave oven (Midea M1-L213B) with a frequency of 2.45 GHz and a power of 700 W. Two SiO_2/Si substrates were stacked together to form a confined space, and the precursors $BiCl_3$ powders were located between the silicon substrates. Then they were placed at the center of microwave and on high (100%) for 1-3 minutes. After the heating, we wear heat protective gloves to take out the samples and place them under running water to remove unreacted $BiCl_3$ powder. Finally, the final product was dried by nitrogen.

4.2 | Characterizations of 2D BiOCl crystals

The as-obtained BiOCl platelets were further characterized by optical microscopy (Olympus BX53M), AFM (Asylum Research Cypher Scanning Probe Microscope system with a tapping mode), SEM (JEOL JSM-7600F), XRD (Rigaku DMAX 2500), RM (WITEC alpha 300R Confocal Raman system using a 532 nm laser as the excitation source), UV-vis spectra (PerkinElmer Lambda 950 UV-vis spectrometer), and XPS (Kratos AXIS Supra spectrometer with a monochromatic Al K-alpha source). ADF-STEM imaging was conducted on an aberration-corrected JEOL ARM-200F equipped with a cold field emission gun, operating at 80 kV, and an advanced STEM corrector probe corrector.

4.3 | PS-assisted transfer of BiOCl onto a fused quartz substrate

PS was first spin-coated on the BiOCl on the SiO_2/Si substrate at 2000 rpm for 60 seconds and then baked at 90°C for 10 minutes. Then, the BiOCl supported by the PS film was peeled off from the SiO_2/Si substrate by tweezers under a drop of DI water. Next, it was transferred onto the fused quartz substrate and dried at 80°C for 1 hour. Finally, the PS film was removed by immersing into toluene for 24 hours, and then successfully transferred the BiOCl samples were dried by nitrogen gas.

4.4 | Device fabrications and measurements

First, the BiOCl flakes grown on SiO_2/Si substrate were spin-coated with 950 K PMMA (MicroChem) at 3000 rpm for 1 minute and baked on a 120°C hotplate for 5 minutes. Then, the BiOCl FET devices were fabricated by standard optical lithography and deposited Ti/Au (20/80 nm) as contact electrodes using electron-beam evaporation. The final devices were annealed for 2 hours with the protection of nitrogen in order to remove resist residues and enhance the metallic contacts.

The electrical characteristics were examined by a semiconductor analyzer (Agilent, B1500A). The photoresponsivity measurement was performed in a digital deep level transient spectroscopy (BIORAD) system with an externally triggerable high power picosecond laser (versatile picosecond laser module from PICOQUANT) by two-pulse photocurrent correlation experiment. The two 266 nm optical pulses from an 80-MHz repetition rate laser were mechanically chopped at 1.85 KHz and then split into two pulses by a 50/50 beam splitter and cross-polarized to minimize interference and focused onto the devices using a ×100 objective lens. The time delay between the two pulses was controlled by a linear translation stage. The photocurrent was collected by a lock-in amplifier with a 5-MΩ input resistance (SR830). Noise spectra are acquired by a spectrum analyzer (Keysight M9018A) with biased supplied by Agilent 1500A at ambient conditions.

4.5 | Calculation of response time

The responsivity of the detector is determined by eliminating the dark current from the current when the light was focused on the sample and calculated as I_{ph} ($I_{ph} = I_{lluminated} - I_{dark}$). Then, the responsivity (R) is calculated by $R = I_{ph}/P_a$, where P_a is the laser power illuminated on the active area of the detector and is calculated by $P_a = P_t \times S_0/S_t$ (P_t is the total laser power measured by the power meter, S_o is the area of the device, and S_t is the area of the laser spot).

ACKNOWLEDGMENTS

This work was supported by the Singapore National Research Foundation under NRF RF Award No. NRF-RF2013-08. MOE Tier 1 RG7/18, MOE Tier 2 MOE2015-T2-2-007, MOE2016-T2-2-153, MOE2017-T2-2-136, MOE Tier 3 MOE2018-T3-1-002, AcRF Tier 2 MOE2017-T2-2-002, NRF2017-NRF-ANR002 2DPS, and A*Star QTE program. Dan Tian thanks the National Nature Science Foundation of China (Grant No. 21601086) and the Natural Science Foundation of Jiangsu Province (BK20160994) for financial support.

CONFLICT OF INTEREST

The authors declare no conflict of interest.

ORCID

Zheng Liu https://orcid.org/0000-0002-8825-7198

REFERENCES

1. Novoselov KS, Geim AK, Morozov SV, et al. Electric field effect in atomically thin carbon films. *Science*. 2004;306:666-669.
2. Geim AK, Novoselov KS. The rise of graphene. *Nat Mater*. 2007; 6:183-191.
3. Zhou J, Lin J, Huang X, et al. A library of atomically thin metal chalcogenides. *Nature*. 2018;556:355-359.
4. Liu F, You L, Seyler KL, et al. Room-temperature ferroelectricity in $CuInP_2S_6$ ultrathin flakes. *Nat Commun*. 2016;7:12357.
5. Gao T, Zhang Q, Li L, et al. 2D ternary chalcogenides. *Adv Opt Mater*. 2018;6:1800058.
6. Wang F, Shifa TA, Yu P, et al. New frontiers on van der Waals layered metal phosphorous trichalcogenides. *Adv Funct Mater*. 2018;28:1802151.
7. Kim SY, Kim Y, Kang C-J, et al. Layer-confined excitonic insulating phase in ultrathin Ta_2NiSe_5 crystals. *ACS Nano*. 2016;10: 8888-8894.

8. Wu J, Yuan H, Meng M, et al. High electron mobility and quantum oscillations in non-encapsulated ultrathin semiconducting Bi_2O_2Se. *Nat Nanotechnol*. 2017;12:530-534.
9. Gong C, Li L, Li Z, et al. Discovery of intrinsic ferromagnetism in two-dimensional van der Waals crystals. *Nature*. 2017;546:265-269.
10. Deng Y, Yu Y, Song Y, et al. Gate-tunable room-temperature ferromagnetism in two-dimensional Fe_3GeTe_2. *Nature*. 2018;563:94-99.
11. Wang F, Gao T, Zhang Q, et al. Liquid-alloy-assisted growth of 2D ternary $Ga_2In_4S_9$ toward high-performance UV photodetection. *Adv Mater*. 2019;31:1806306.
12. Cheng H, Huang B, Dai Y. Engineering BiOX (X = Cl, Br, I) nanostructures for highly efficient photocatalytic applications. *Nanoscale*. 2014;6:2009-2026.
13. Li H, Li J, Ai Z, Jia F, Zhang L. Oxygen vacancy-mediated photocatalysis of BiOCl: reactivity, selectivity, and perspectives. *Angew Chem Int Ed*. 2018;57:122-138.
14. Li J, Li H, Zhan G, Zhang L. Solar water splitting and nitrogen fixation with layered bismuth oxyhalides. *Acc Chem Res*. 2017;50:112-121.
15. Zeng W, Li J, Feng L, et al. Synthesis of large-area atomically thin BiOI crystals with highly sensitive and controllable photodetection. *Adv Funct Mater*. 2019;29:1900129.
16. Cui D, Wang L, Xu K, et al. Band-gap engineering of BiOCl with oxygen vacancies for efficient photooxidation properties under visible-light irradiation. *J Mater Chem A*. 2018;6:2193-2199.
17. Wosylus A, Hoffmann S, Schmidt M, Ruck M. In-situ study of the solid-gas reaction of $BiCl_3$ to BiOCl via the intermediate hydrate $BiCl_3{\cdot}H_2O$. *Eur J Inorg Chem*. 2010;2010:1469-1471.
18. Sun Y, Yang L, Xia K, et al. "Snowing" graphene using microwave ovens. *Adv Mater*. 2018;30:1803189.
19. Ai L, Zeng Y, Jiang J. Hierarchical porous BiOI architectures: facile microwave nonaqueous synthesis, characterization and application in the removal of Congo red from aqueous solution. *Chem Eng J*. 2014;235:331-339.
20. Seddigi ZS, Gondal MA, Baig U, et al. Facile synthesis of light harvesting semiconductor bismuth oxychloride nano photocatalysts for efficient removal of hazardous organic pollutants. *PLOS One*. 2017;12:0172218.
21. Di J, Chen C, Yang S-Z, et al. Defect engineering in atomically-thin bismuth oxychloride towards photocatalytic oxygen evolution. *J Mater Chem A*. 2017;5:14144-14151.
22. Zhou S, Gan L, Wang D, Li H, Zhai T. Space-confined vapor deposition synthesis of two dimensional materials. *Nano Res*. 2018;11:2909-2931.
23. Zhou S, Wang R, Han J, et al. Ultrathin non-van der Waals magnetic Rhombohedral Cr_2S_3: space-confined chemical vapor deposition synthesis and raman scattering investigation. *Adv Funct Mater*. 2019;29:1805880.
24. Fu Q, Zhu C, Zhao X, et al. Ultrasensitive 2D Bi_2O_2Se phototransistors on silicon substrates. *Adv Mater*. 2019;31:1804945.
25. Zhao R, Li X, Zhai Y, et al. Effect of chlorine source on the morphology of flower-like BiOCl and its photocatalytic activity. *J Adv Oxid Techno*. 2015;18:353-360.
26. Zhao X, Ning S, Fu W, Pennycook SJ, Loh KP. Differentiating polymorphs in molybdenum disulfide via electron microscopy. *Adv Mater*. 2018;30:1802397.
27. Krivanek OL, Chisholm MF, Nicolosi V, et al. Atom-by-atom structural and chemical analysis by annular dark-field electron microscopy. *Nature*. 2010;464:571-574.
28. Yin J, Tan Z, Hong H, et al. Ultrafast and highly sensitive infrared photodetectors based on two-dimensional oxyselenide crystals. *Nat Commun*. 2018;9:3311.
29. Xia F, Mueller T, Y-m L, et al. Ultrafast graphene photodetector. *Nat Nanotechnol*. 2009;4:839-843.
30. Wang H, Zhang C, Chan W, Tiwari S, Rana F. Ultrafast response of monolayer molybdenum disulfide photodetectors. *Nat Commun*. 2015;6:8831.
31. Monroy E, Omn s F, Calle F. Wide-bandgap semiconductor ultraviolet photodetectors. *Semicond Sci Technol*. 2003;18:33-51.
32. Yu X, Yu P, Wu D, et al. Atomically thin noble metal dichalcogenide: a broadband mid-infrared semiconductor. *Nat Commun*. 2018;9:1545.

SUPPORTING INFORMATION

Additional supporting information may be found online in the Supporting Information section at the end of this article.

How to cite this article: Kang L, Yu X, Zhao X, et al. Space-confined microwave synthesis of ternary-layered BiOCl crystals with high-performance ultraviolet photodetection. *InfoMat*. 2020;2:593–600. https://doi.org/10.1002/inf2.12033